Research Article | Vol. 31, No. 18 / 28 Aug 2023 / Optics Express 29392
Optics EXPRESS

Embedded silicon gratings for high-efficiency light-chip coupling to thin film silicon nitride waveguides

PRAVIN RAWAT,[†] SIDDHARTH NAMBIAR,[†] P. VENKATACHALAM,[†] RADHAKANT SINGH,[†] AND SHANKAR KUMAR SELVARAJA[*]

Center for Nano Science and Engineering, Indian Institute of Science, Bangalore, India
[†]Equal contribution.
http://www.cense.iisc.ac.in/shankarks/
[*]*shankarks@iisc.ac.in*

Abstract: Thin film silicon nitride (<150 nm) waveguide has emerged as a dominant ultra-low-loss platform for many loss-critical applications. While thin-film silicon nitride propagation loss is a crucial characteristic, coupling light between an optical fiber and the waveguide is still challenging. While the larger mode size of the decoupled thin waveguide offers better coupling than a highly-confined waveguide, the coupling efficiency is still sub-optimal. The poor diffraction efficiency of such thin films limits the scope of implementing standalone surface gratings. We demonstrate an efficient way to couple into thin film silicon nitride waveguides using amorphous silicon strip gratings. The high contrast gratings provide an efficient means to boost the directionality from thin films leading to an enhanced coupling performance. In addition, we incorporate a bottom reflector to further improve the coupling. We present an optimal design for uniform strip gratings with a maximum coupling efficiency of -1.7 dB/coupler. We achieved a maximum coupling efficiency of -0.28 dB/coupler by engineering the scattering strength along the grating through apodization. We have experimentally shown the highest coupling efficiency reported yet of -2.22 dB/coupler and -1.84 dB/coupler for uniform and apodized grating couplers in the C-L band. We present a detailed design strategy, simulation, fabrication and characterization data on the effect of various parameters on the coupling efficiency.

1. Introduction

Photonic integrated circuits (PICs) based on silicon photonics are now key technology enablers for a wide range of applications from high-speed data communications to high-performance computing and on-chip sensing. Among the various PIC platforms, the silicon-on-insulator (SOI) stack continues to be the workhorse with an increasing complementary footprint of silicon nitride (SiN) due to its wideband transparency and photonic functionalities [1]. Recently there has been a growing interest towards developing low-loss photonic interconnects based on thin-film silicon nitride (*TFSiN*). This platform consists of low aspect ratio core waveguides with thicknesses between 40 and 200 nm. A characteristic feature of *TFSiN* is the low material-induced propagation loss due to the extremely low mode-field confinement in the waveguide core. Depending on the core waveguide geometry, propagation losses can vary between 0.1-30 dB/m [2–5]. These losses are significantly lower than SOI PICs and platforms based on moderately thick SiN grown using standard chemical vapour deposition processes. Such *TFSiN*-based low-loss interconnects are being explored for numerous on-chip applications such as true time delay lines for microwave photonics [6–8], ultra-high Q-factor cavity resonators for frequency combs [9], miniaturized spectrometers for astro-photonics [10], four-wave mixing [11] as well as narrow linewidth Brillouin lasers [12].

#488999 https://doi.org/10.1364/OE.488999
Journal © 2023 Received 1 Mar 2023; revised 1 Jun 2023; accepted 11 Jun 2023; published 18 Aug 2023

Optics EXPRESS

The conventional approach to enable fibre-chip coupling to such weakly guiding films is through in-plane edge-couplers. For *TFSiN* waveguides, a large mode field of the fundamental mode with silicon dioxide cladding means better overlap with the fibre mode, thereby leading to relaxed alignment tolerances for edge-couplers compared to high confinement platforms such as 400 nm thick *SiN* and SOI. Nevertheless, edge-couplers also require post-fabrication steps like facet polishing and are incompatible with wafer-scale testing. On the other hand, implementing out-of-plane surface gratings on such low-index contrast thin films presents a design challenge due to the extremely low diffraction efficiency, leading to poor directionality and thereby impacting coupling performance.

One way to boost the diffraction efficiency is to use a composite grating stack composed of a high-index material like amorphous silicon ($a-Si$). Dual-layer gratings composed of such hybrid stacks have already been demonstrated on the SiN-on-SOI platform [13,14]. However, grating coupling to *TFSiN* waveguides are emerging to appear [5,15]. A critical limiting factor in fabricating dual-layer designs is the need for precise layer alignment and surface planarization. In this work, we propose and experimentally demonstrate a Si-strip grating for high-efficiency coupling to *TFSiN* waveguides. The grating teeth consist of a fully etched, single-layer $a-Si$ grating embedded in the *TFSiN* waveguiding layer. Different design optimization methods are explored to enhance coupling, including incorporating a bottom reflector stack and applying an apodization function to engineer the strip geometry. We present the best coupler efficiency of -0.28 dB/coupler with an optimized grating design. We experimentally demonstrate a maximum coupling efficiency of -1.84 dB/coupler between a single-mode optical fibre and a 125 nm thin *SiN* single-mode waveguide. The reported efficiency is the best reported yet to our knowledge.

2. Design and simulation

2.1. Waveguide design

Thin-film *SiN* waveguides currently cover many waveguide thicknesses and widths. The choice of thickness has implications on the device performance, layout, and process technology. This work uses a 125 nm thick *SiN* layer as a demonstration platform. Figure 1(a) summarises the modal simulation of *TFSiN* waveguide. Figure 1(a) shows the waveguide effective index as a function of waveguide width. The modal calculations were performed using finite difference eigenmode solver available in MODE package of Ansys Lumerical. The mode field intensity of the propagating modes is shown as an inset. The bottom cladding thickness is estimated from the 1/e field decay length in the vertical direction. For a waveguide width of 3 μm, a thickness of 1.8 μm is sufficient to avoid substrate leakage (Fig. 1(b)).

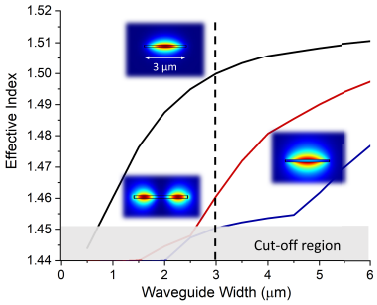

(a) Effective index of propagating mode in a 125 nm thin SiN.

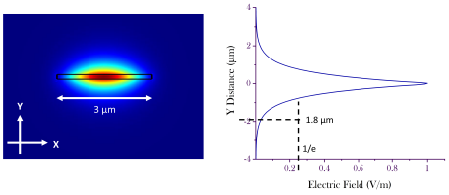

(b) Vertical field decay of the fundamental TE propagating mode.

Fig. 1. Summary of modal calculation.

Optics EXPRESS

In addition to the waveguide dimensions, the bend loss of the *TFSiN* waveguide is calculated. Figure 2(a) shows the bend loss as a function of the bending radius, which was simulated using the Film Mode Matching Method of FIMMWAVE package from Photon Design, in which the desired curvature is specified to obtain loss value for the respective curvature. A bending radius over 200 μm is desirable for achieving a low-loss circuit. Unlike the tightly confined waveguides, the low propagation loss in straight waveguides comes at the cost of larger bend radii.

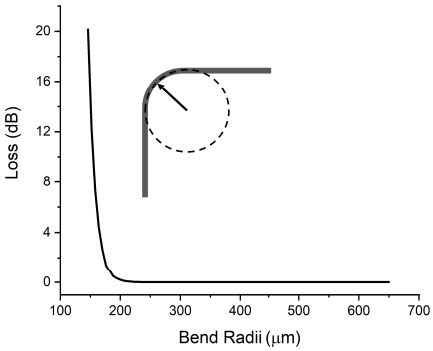

(a) Effect of bend radius on the bent loss.

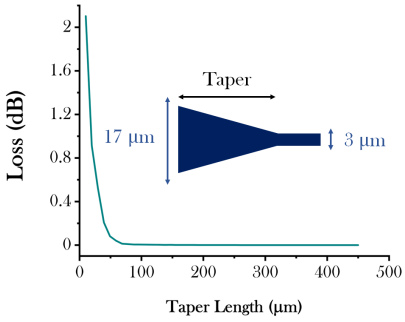

(b) Effect of taper length on the taper-to-waveguide loss (simulated using two dimensional finite difference time domain (2D-FDTD) solver from Ansys Lumerical).

Fig. 2. Optimisation of bend and taper loss.

While building a circuit with grating couplers, the grating diffraction footprint/area matches the fibre mode dimension. Thus, the grating should be made on a wider waveguide. The wider waveguide should be tapered down to the desired waveguide width. A taper with minimal propagation loss is desired to exploit the low-loss potential of the *TFSiN* platform. Figure 2(b) shows the minimum length required for a low-loss taper between a broad 17 μm and a 3 μm wide waveguide. We observe that a taper length over 60 μm would result in a nearly loss-less transition.

2.2. Grating design

Figure 3 presents a schematic of the proposed grating coupling structure. The waveguide layer is 125 nm thick *SiN* embedded in a top and bottom silicon dioxide cladding. Embedded silicon grating strips define the grating. Initially, we rationalize the need for a diffraction enhancement. We introduce an embedded amorphous-Si ($a-Si$) grating to improve the diffraction efficiency. We present a detailed design and simulation of the proposed embedded-Si as a uniform and apodized grating configuration (Fig. 3). Taking into account the topographical impact of *TFSiN* waveguide on the embedded Si strip, the grating constructor can be expressed as:

$$\begin{aligned} N\Lambda_u = &\sum_{i=1,F_{u1},t=t_1}^{i=N,F_{u1}} [F_i\Lambda_u + (1-F_i)\Lambda_u] \\ &+ \sum_{i=1,F_{u2},t=t_1+t_2}^{i=N,F_{u2}} [F_i\Lambda_u + (1-F_i)\Lambda_u] \end{aligned} \tag{1}$$

where F_{u1} is the constant fill-factor of the strip gratings, and $F_{u2} = (F_{u1} + 2t_2/\Lambda_u)$ is the constant fill-factor of the *TFSiN* topography. N defines the number of periods, and Λ_u is the uniform grating period. The simulations are performed using the 2D FDTD method. The parameters t_1 and t_2 are thicknesses of $a-Si$ strip and *TFSiN* films, respectively. The thickness of *TFSiN* is

Optics EXPRESS

fixed at 125 nm. In the case of *SiN* only gratings, the second part of Eq. (1) applies with $t_1 = 0$. The refractive indices of *TFSiN*, $a - Si$, and SiO_2 are taken from the measured ellipsometry to be 2.015, 3.48 and 1.45, respectively.

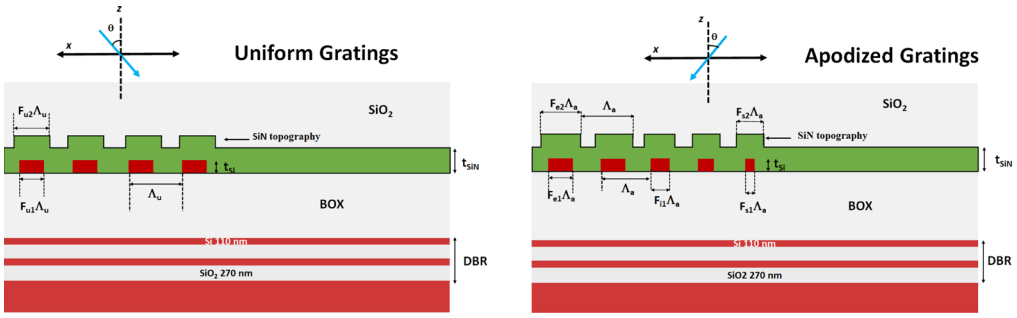

Fig. 3. 2D schematic of the uniform grating and apodized grating designs with all parameters used in simulations.

The coupling efficiency of the grating is simulated by launching a Gaussian mode with a 10.4 μm mode-field diameter over the grating. The coupling efficiency is calculated, through a power monitor placed across the waveguide, 13 μm from grating, to eliminate radiative coupling. The minimum mesh step was taken was 10 nm.

Effect of grating parameters such as period, fill-factor $a - Si$ thickness, BOX thickness and the incident angle on the coupling efficiency is performed. For standalone *SiN* gratings, a peak coupling efficiency of less than 20 % is observed (Fig. 4). The low coupling efficiency is primarily due to poor grating strength. The coupling efficiency is improved by increasing the scattering strength of the grating with the thickness of the $a - Si$ thickness. However, the efficiency drops beyond 70 nm due to higher reflection loss. Thus, the grating strength should be optimal for scattering and reflection. Maximum efficiency of 55 % is achieved for an $a - Si$ strip thickness of 70 nm. The optimal grating period Λ_u, no. of gratings N and fill-factor are 970 nm, 21 and 40 %, respectively with the peak angle of incidence θ being 7° for a 70 nm thick $a - Si$.

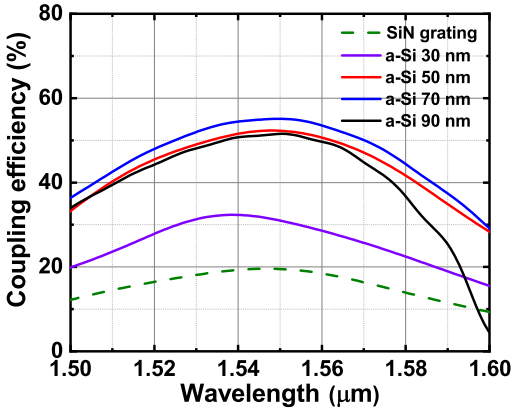

Fig. 4. Effect of $a - Si$ thickness on the coupling efficiency. Here no $a - Si$ corresponds to standalone fully etched *SiN* gratings. The optimum period for a standalone grating and $a - Si$ = 30, 50, 70, and 90 nm are 1.17, 1.05, 1.01, 0.97 and 0.95 μm, respectively.

A significant amount of light gets leaked into the substrate for the $a - Si$. Incorporating a bottom reflector can redirect the downward scattered light upwards, boosting directionality and

Optics EXPRESS

thereby coupling efficiency, as shown in many previous works [16,17]. Such a reflector can be a highly reflective single metal film or a dielectric stack of distributed Bragg reflectors (DBR). Here we consider a stack of 110/270 nm $a\text{-}Si/SiO_2$. In Fig. 5(a) and 5(b), the simulated coupling efficiency is depicted as a function of period and angle for an $a-Si$ strip grating of 70 nm thickness with a DBR substrate. Peak efficiency in C-band is 74 % (-1.3 dB), peaking at 1546 nm wavelength with a 1dB bandwidth of 85 nm. Figure 6 shows the effect of bottom-oxide (BOX) cladding thickness on the coupling efficiency for the optimized grating design. We choose 1.8 μm for the DBR stack based on the optimal phase matching thickness. For a waveguide, the BOX layer should be optically isolated from the substrate to avoid substrate leakage. From Fig. 1(b), it is clear that a substrate isolation of 1.8 μm is sufficient to avoid substrate leakage. However, a thicker phase-matching BOX could be used (Fig. 6). The reported efficiency is the best reported yet to our knowledge.

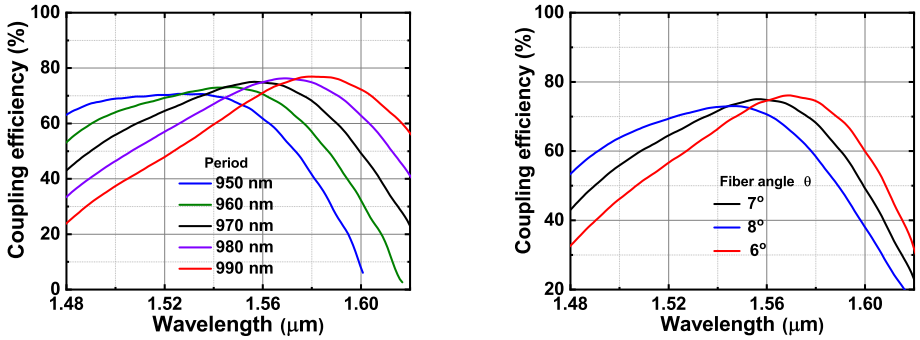

Fig. 5. Effect of (a) grating period and (b) incident angle on the coupling efficiency of uniform grating with bottom reflector with θ = 7deg and Λ_u of 970 nm, respectively.

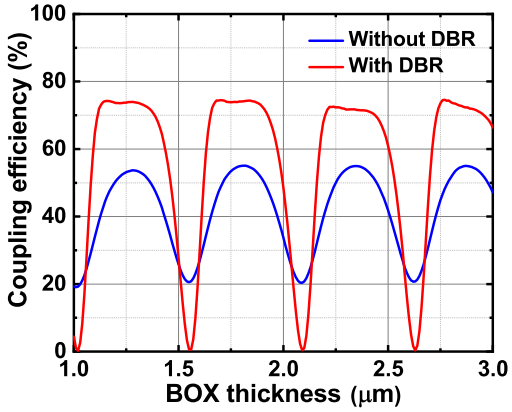

Fig. 6. Effect of bottom oxide thickness on the coupling efficiency of a uniform grating with and without a DBR stack. The plot shows maximum efficiency for Λ_u = 970 nm and $\theta = 7^\circ$

Further improvement in coupling efficiency can be achieved through the diffraction field optimization with grating apodization [18,19]. In the above design, we apply an apodization function (AF), where the period, incident angle and fill-factor are varied while the BOX thickness

Optics EXPRESS

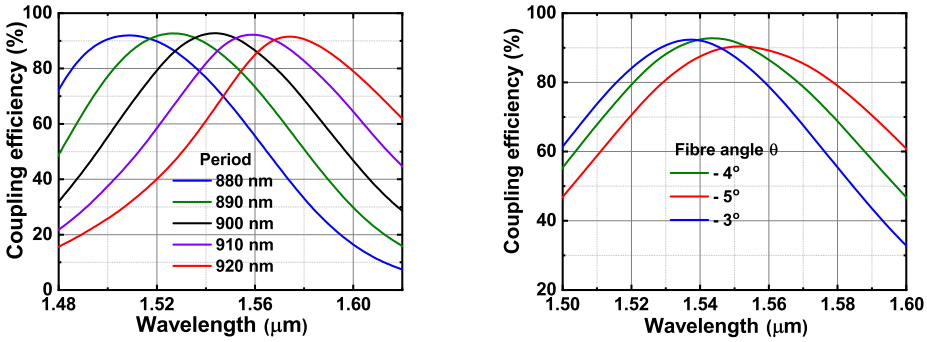

(a) (b)

Fig. 7. Effect of (a) grating period and (b) incident angle on the coupling efficiency of uniform grating with bottom reflector with θ = 7deg and Λ_u of 970 nm, respectively.

is fixed. On applying the AF, the modified (1) is expressed as,

$$N\Lambda_a = \sum_{i=1,F_{s1},t=t_1}^{i=N,F_{e1}} [F_i\Lambda_a + (1-F_i)\Lambda_a] + \sum_{i=1,F_{s2},t=t_1+t_2}^{i=N,F_{e2}} [F_i\Lambda_a + (1-F_i)\Lambda_a]. \quad (2)$$

Where Λ_a is the apodized grating period, F_{s1} and F_{e1} are the start and end fill-factors of the strip gratings. Similarly, $F_{s2} = (F_{s1} + 2t_2/\Lambda_a)$ and F_{e2} are the start and end fill-factors of the *TFSiN* topography. Figure 3 illustrates the apodized grating design. The optimized N, F_{s1} and F_{e1} are 27, 0.55 and 0.07, respectively. The coupling efficiency as a function of period and angle is shown in Fig. 7(b). Peak efficiency in C-band is 92.7 % (-0.28 dB) at 1544 nm, for a period of 900 nm and angle of -4°. Figure 8 compares the emitted electric field intensities of apodized and

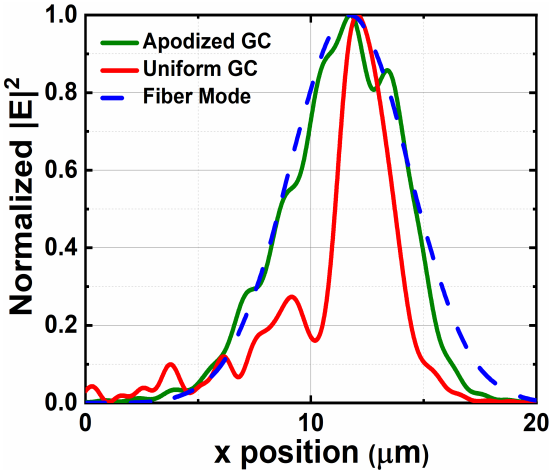

Fig. 8. Normalised scattered electric field intensity for uniform, apodized gratings and a Gaussian source, along the propagation axis x.

Optics EXPRESS

uniform gratings. The improvement in coupling efficiency of 18 % over uniform gratings can be attributed to the improved overlap with the Gaussian mode.

3. Test device

Figure 9 shows a schematic of the test circuits used for the demonstration. We use two types of grating test devices; uniform grating and apodized grating. The uniform grating test circuit is constructed with two identical gratings at the ends connected through a broad patch waveguide in one of the configurations and through adiabatic waveguide tapers, a straight waveguide and an S-bend in another configuration. Figure 9 shows the test circuit schematic. Similarly, the apodized grating is designed with a waveguide taper. However, since the coupling angle is negative, as depicted in Fig. 9, a C-bend is used to route the light.

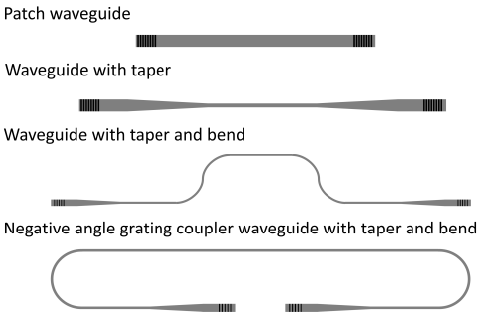

Fig. 9. Schematic of test structures.

4. Fabrication and characterization

The device fabrication is done on a clean silicon wafer. Figure 10 shows an overview of the fabrication process. The DBR stack is first formed by successive deposition of $a-Si$ and SiO_2 using a plasma-enhanced chemical vapour deposition (PECVD) process. A layer thickness of 110 nm and 270 nm is chosen as the optical thickness of $a-Si$ and SiO_2, respectively. Following the mirror, a 1.8 μm of PECVD SiO_2 is deposited as the bottom cladding. A 70 nm of PECVD $a-Si$ is deposited for grating definition. The grating patterning uses electron-beam lithography, and an inductively-coupled plasma reactive ion etch (ICP-RIE) process. The patterning process is optimized for both uniform and apodized grating test structures. The grating is defined by fully etching the 70 nm thick $a-Si$ using fluorine-based etch chemistry, landing on SiO_2. A blanket 125 nm thick PECVD SiN is deposited following the grating patterning. The waveguides are patterned using optical lithography and the ICP-RIE process. The patterned waveguides are covered with 1.9 μm thick PECVD SiO_2. Figure 11(a), 11(b), and 11(c) summarises the fabrication process result.

The fabricated devices are characterized using a tunable laser (Keysight 81960A) with a photodetector module (81636B) in the C-L band. Single mode fibers (SMF) are used to connect the laser to polarization controllers, which are in turn connected to SMF mounted on a variable stage goniometer (for angle sweeping). The output fibers from the stage are connected to the photodetector. The coupling efficiency is calculated by normalizing the measured transmission through the device with the source spectrum. The measured coupling efficiency of uniform gratings with bottom mirror is shown in Fig. 12(a) and 12(b). Peak efficiency and wavelengths in the C-L band are measured to be -3.58 dB at 1561 nm, -2.37 dB at 1570 nm and -2.22 dB at 1601 nm for grating periods of 940 nm, 950 nm and 960 nm. The corresponding 1-dB bandwidths

Optics EXPRESS

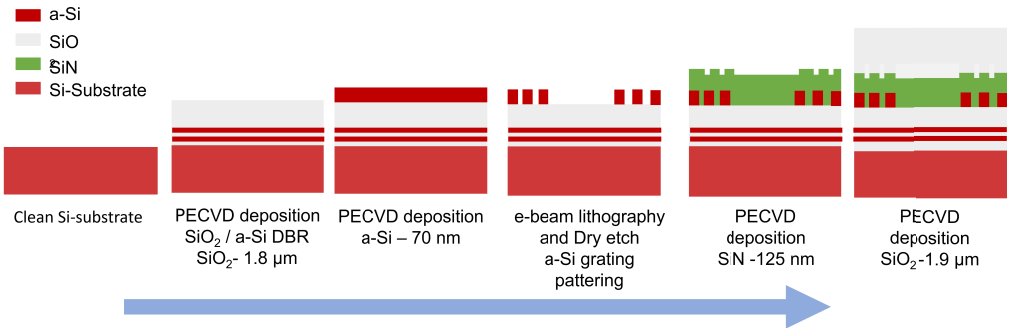

Fig. 10. Fabrication process overview.

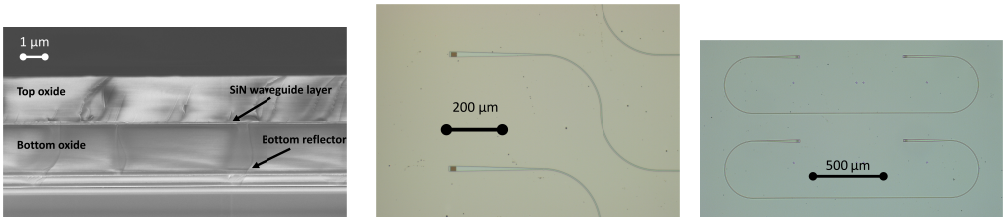

(a) (b) (c)

Fig. 11. (a) shows cross-sectional SEM image of the deposited stack with a SBR and top cladding. (b) shows a top down image of uniform gratings with S-bend coupled to straight waveguides.(c) shows top-down image of apodized gratings with C bends coupled to straight waveguides.

for these periods are measured to be 39 nm, 50 nm and 49 nm, respectively. The peak angle of incidence is observed at 10 °, which is higher than that observed in simulations. This excess loss of tapers and bends can be extracted by measurement of patch grating efficiency (for uniform designs as shown in Fig. 9). Figure 13 shows the normalized fibre-to-fibre transmission loss of the test device with patch, taper, and bend waveguide. We estimate a bend loss of 0.14 dB/90° for a bend radius of 200 μm, limited by practical sample size but is not fundamental. The loss could be reduced by using a larger radius 660 μm. However, We did not observe additional loss due to the waveguide tapers.

Figure 14 shows the effect of the grating period and fibre angle on the coupling efficiency of the apodized gratings. The coupling efficiency includes the taper, waveguide and bend loss. A peak coupling efficiency of -2.12 dB is measured for a period of 890 nm and a fibre angle θ of -6°. The efficiency includes excess loss. We estimate a coupling efficiency of -1.84 dB/coupler after deducing a minimum excess loss due to the bends, including taper loss. The deviation from the simulated optimal period, incidence angle and bandwidth for both uniform and apodized gratings could be due to localized variation in fill factor and *a-Si* grating thickness. Since the device is fabricated on an oxide substrate, SEM imaging of the device features is extremely difficult due to electron charging. Table 1 provides a performance comparison for grating couplers reported for *TFSiN* platform.

Optics EXPRESS

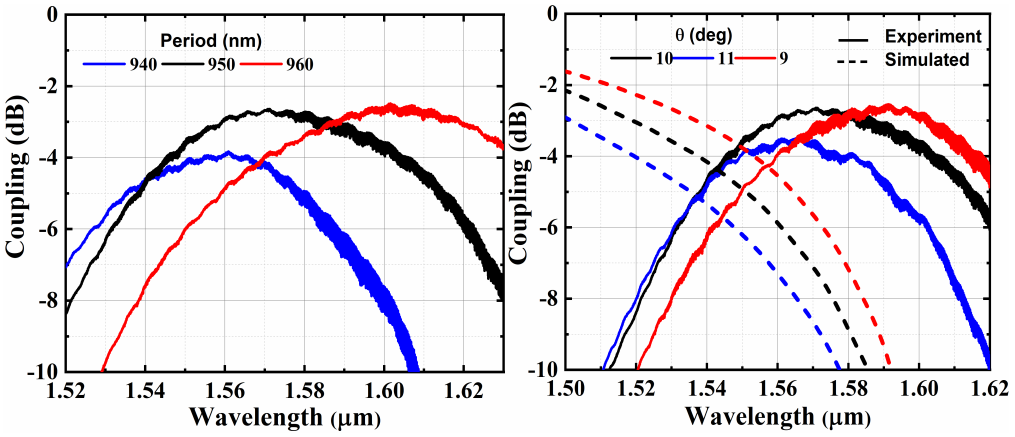

(a) (b)

Fig. 12. Measured coupling efficiency of a uniform grating for (a) various periods Λ_u at θ = 10° and (b) various θ at Λ_u = 950 nm. The dashed lines depict the simulated values for corresponding period

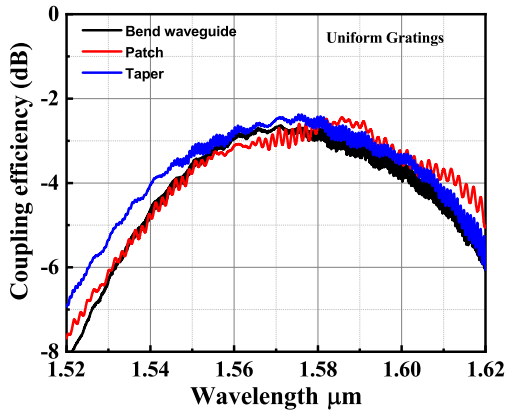

Fig. 13. Comparison of measured fibre-chip coupling efficiency for a uniform grating with bends, linear tapered waveguides and patch waveguides for a grating period of 950 nm.

Table 1. Comparison of grating couplers in thin *SiN* platform in literature.

Ref	SiN thickness (nm)	Coupling efficiency (dB)		Bandwidth (nm)		Etch steps	Grating type	Bottom reflector
		Simulated	Measured	1-dB	3-dB			
[5]	100		-5		75	2	Uniform	No
[15]	150	-0.75	NA	57		2	Apodized	No
This work	125	-1.3	-2.22	50		1	Uniform	Yes
This work	125	-0.28	-1.84	46		1	Apodized	Yes

Optics EXPRESS

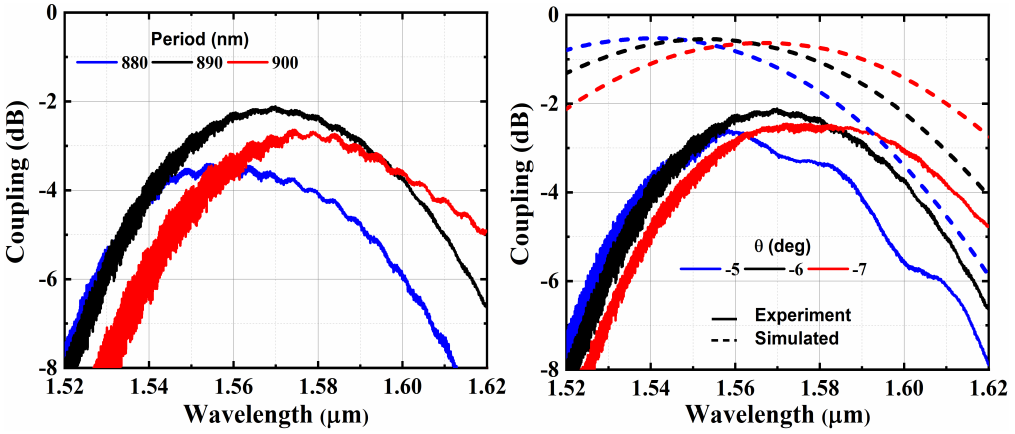

Fig. 14. Measured coupling efficiency of an apodized grating as a function of period Λ_a at θ = -6°, and (b) θ at Λ_a = 890 nm with dashed lines showing the corresponding simulated values.

5. Conclusion

We report high-efficiency gratings for coupling to thin-film silicon nitride waveguide. The gratings comprise a single fully etched layer of embedded *Si* strip. The strong diffraction of high contrast strip-gratings enables higher coupling when compared to standalone *SiN* gratings. A combination of bottom reflector and grating apodization achieves a high experimental coupling efficiency of -1.84 dB per coupler. The proposed design offers a versatile and scalable approach for facilitating fibre-chip coupling for a low-loss thin film silicon nitride platform.

Funding. Ministry of Education, India; Ministry of Electronics and Information technology.

Acknowledgement. SKS thanks Professor Ramakrishna Rao chair fellowship. All the authors acknowledge NNfC (National Nano fabricaiton Centre) and MNCF (Micro and Nano Characterisation Facility) at CeNSE, IISc for the facility support.

Disclosures. The authors declare no conflicts of interest.

Data availability. Data underlying the results presented in this paper are not publicly available at this time but may be obtained from the authors upon reasonable request.

References

1. C. Xiang, W. Jin, and J. E. Bowers, "Silicon nitride passive and active photonic integrated circuits: trends and prospects," Photonics Res. **10**(6), A82–A96 (2022).
2. J. F. Bauters, M. J. R. Heck, D. D. John, J. S. Barton, C. M. Bruinink, A. Leinse, R. G. Heideman, D. J. Blumenthal, and J. E. Bowers, "Planar waveguides with less than 0.1 dB/m propagation loss fabricated with wafer bonding," Opt. Express **19**(24), 24090–24101 (2011).
3. T. A. Huffman, G. M. Brodnik, C. Pinho, S. Gundavarapu, D. Baney, and D. J. Blumenthal, "Integrated resonators in an ultralow loss Si3N4/SiO2 platform for multifunction applications," IEEE J. Sel. Top. Quantum Electron. **24**(4), 1–9 (2018).
4. K. Shang, S. Pathak, B. Guan, G. Liu, and S. J. B. Yoo, "Low-loss compact multilayer silicon nitride platform for 3D photonic integrated circuits," Opt. Express **23**(16), 21334–21342 (2015).
5. B. Chmielak, S. Suckow, J. Parra, V. C. Duarte, T. Mengual, M. A. Piqueras, A. L. Giesecke, M. C. Lemme, and P. Sanchis, "High-efficiency grating coupler for an ultralow-loss Si3N4-based platform," Opt. Lett. **47**(10), 2498–2501 (2022).
6. C. G. H. Roeloffzen, L. Zhuang, C. Taddei, A. Leinse, R. G. Heideman, P. W. L. van Dijk, R. M. Oldenbeuving, D. A. I. Marpaung, M. Burla, and K. J. Boller, "Silicon nitride microwave photonic circuits," Opt. Express **21**(19), 22937–22961 (2013).
7. X. Wang, L. Zhou, R. Li, J. Xie, L. Lu, K. Wu, and J. Chen, "Continuously tunable ultra-thin silicon waveguide optical delay line," Optica **4**(5), 507–515 (2017).

Optics EXPRESS

8. R. L. Moreira, J. Garcia, W. Li, J. Bauters, J. S. Barton, M. J. R. Heck, J. E. Bowers, and D. J. Blumenthal, "Integrated ultra-low-loss 4-bit tunable delay for broadband phased array antenna applications," IEEE Photonics Technol. Lett. **25**(12), 1165–1168 (2013).
9. D. T. Spencer, J. F. Bauters, M. J. R. Heck, and J. E. Bowers, "Integrated waveguide coupled Si3N4 resonators in the ultrahigh-Q regime," Optica **1**(3), 153–157 (2014).
10. P. Gatkine, S. Veilleux, Y. Hu, J. Bland-Hawthorn, and M. Dagenais, "Arrayed waveguide grating spectrometers for astronomical applications: new results," Opt. Express **25**(15), 17918–17935 (2017).
11. C. J. Krückel, V. Torres-Company, P. A. Andrekson, D. T. Spencer, J. F. Bauters, M. J. R. Heck, and J. E. Bowers, "Continuous wave-pumped wavelength conversion in low-loss silicon nitride waveguides," Opt. Lett. **40**(6), 875–878 (2015).
12. S. Gundavarapu, G. M. Brodnik, M. Puckett, T. Huffman, D. Bose, R. Behunin, J. Wu, T. Qiu, C. Pinho, N. Chauhan, J. Nohava, P. T. Rakich, K. D. Nelson, M. Salit, and D. J. Blumenthal, "Sub-hertz fundamental linewidth photonic integrated brillouin laser," Nat. Photonics **13**(1), 60–67 (2019).
13. W. D. Sacher, Y. Huang, L. Ding, B. J. F. Taylor, H. Jayatilleka, G.-Q. Lo, and J. K. S. Poon, "Wide bandwidth and high coupling efficiency Si3N4-on-SOI dual-level grating coupler," Opt. Express **22**(9), 10938–10947 (2014).
14. P. Xu, Y. Zhang, Z. Shao, L. Liu, L. Zhou, C. Yang, Y. Chen, and S. Yu, "High-efficiency wideband SiNx-on-SOI grating coupler with low fabrication complexity," Opt. Lett. **42**(17), 3391–3394 (2017).
15. V. Vitali, C. Lacava, T. Domínguez Bucio, F. Y. Gardes, and P. Petropoulos, "Highly efficient dual-level grating couplers for silicon nitride photonics," Sci. Rep. **12**(1), 15436 (2022).
16. Y. Ding, C. Peucheret, H. Ou, and K. Yvind, "Fully etched apodized grating coupler on the SOI platform with - 0.58 dB coupling efficiency," Opt. Lett. **39**(18), 5348–5350 (2014).
17. H. Zhang, C. Li, X. Tu, J. Song, H. Zhou, X. Luo, Y. Huang, M. Yu, and G. Q. Lo, "Efficient silicon nitride grating coupler with distributed bragg reflectors," Opt. Express **22**(18), 21800–21805 (2014).
18. S. Nambiar, P. Ranganath, R. Kallega, and S. K. Selvaraja, "High efficiency DBR assisted grating chirp generators for silicon nitride fiber-chip coupling," Sci. Rep. **9**(1), 18821 (2019).
19. S. Nambiar, A. Chatterjee, and S. K. Selvaraja, "Comprehensive grating enabled silicon nitride fiber-chip couplers in the snir wavelength band," Opt. Express **30**(3), 4327–4341 (2022).